

Modeling features in the redshift-space halo power spectrum with perturbation theory

Shi-Fan Chen^a Zvonimir Vlah^b Martin White^a

^aDepartment of Physics, University of California, Berkeley, CA 94720

^bTheory Department, CERN, CH-1211 Geneve 23, Switzerland

E-mail: shifan_chen@berkeley.edu, zvonimir.vlah@cern.ch, mwhite@berkeley.edu

Abstract. We study the ability of perturbative models with effective field theory contributions and infra-red resummation to model the redshift space clustering of biased tracers in models where the linear power spectrum has “features” – either imprinted during inflation or induced by non-standard expansion histories. We show that both Eulerian and Lagrangian perturbation theory are capable of reproducing the Fourier space two-point functions of halos up to the non-linear scale from a suite of 4096^3 particle N-body simulations. This is the first demonstration that perturbative models can accurately fit the redshift-space clustering of biased tracers in N-body simulations of such theories. By comparing different theoretical models and IR resummation schemes we assess the current theoretical uncertainty in predicting power spectra for models with features. Our results suggest that future surveys will be able to detect or tightly constrain features in the primordial spectrum below the one percent level across a wide range of scales.

Keywords: power spectrum – galaxy clustering

Contents

1	Introduction	1
2	N-body simulations	2
3	Feature models	3
3.1	Primordial features	3
3.2	Induced features	4
4	Perturbative model	5
4.1	Overview of Previous Work	5
4.2	Lagrangian IR Resummation and Connection to Earlier Approaches	6
4.3	Redshift-Space Distortions	8
5	Results	9
6	Conclusions	12
A	Saddle-Point Approximation for Nonlinear Dispersions	15
B	GSM vs. moment expansion	16

1 Introduction

Current observations of large-scale structure are consistent with a primordial power spectrum that is featureless, upon which 14 Gyr of evolution imprints two characteristic scales: the horizon at the epoch of matter-radiation equality and the sound horizon of photon-baryon acoustic oscillations prior to recombination [1–3]. However many modifications of the standard model would lead to deviations from this simple picture. Many inflationary models imprint features in the otherwise smooth spectrum of curvature fluctuations at early times (see e.g. refs. [4, 5] for recent reviews and references to the extensive early literature). While these features are in some sense generic, different models predict very different properties for these features, their bandwidth, amplitude and shape. Detection of such features would open new windows into the primordial Universe. In addition, the evolution of these primordial perturbations across 14 Gyr of cosmic history can ‘induce’ features in the observed spectrum. One class of features which has been the focus of intense observational activity are baryon acoustic oscillations [6]. However more generally new types of particle interactions, new energy components or changes in the expansion history can all alter the observed, late-time spectrum in observable ways.

The strongest constraints on primordial features to date come from a combination of cosmic microwave background anisotropies [3, 7] and large-scale structure [8]. This has placed upper limits on the amplitude of features at the several percent level for frequencies in the range $10^2 < \omega < 10^3 h^{-1}\text{Mpc}$ (see previous references for more details). Future large-scale structure

surveys, especially those performed at high redshift over large cosmic volumes, should be able to tighten these constraints significantly [5].

In this paper we investigate the degree to which modern perturbative calculations can quantitatively predict the clustering of biased tracers in redshift space, including the “washing out” of primordial features by mode-coupling associated with non-linear evolution, changes to the broad-band shape of the spectrum by non-linear biasing and the mixing of the velocity and density perturbations through redshift-space distortions. We are not the first authors to address these topics, indeed there is an extensive literature on this topic within the context of baryon acoustic oscillation (BAO) studies (see §4 for references). An important finding of these studies is the existence of $\mathcal{O}(1)$ corrections to features for a wide range of parameters and wavenumbers of interest. This leads one to consider resumming these $\mathcal{O}(1)$ contributions, which arise from the large displacements, a process referred to as IR resummation. One method of deriving the IR resummation process is as a saddle-point approximation to a particular integral (§4). In this paper we pay particular attention to the manner in which IR resummation, mode coupling and the mixing of density and velocity perturbations implied by redshift-space distortions appear in models with features at different scales than BAO, and how IR resummation can deal with features with k -dependent frequency where the choice of saddle is not immediately obvious.

The outline of the paper is as follows. In Section 2 we introduce the particle-mesh simulations that we use to validate our perturbative models. Section 3 describes the specific feature models that we test, which have been chosen to be representative of different classes that appear in the literature, while Section 4 describes the perturbative calculations we investigate. Section 5 presents the comparison between the theory and N-body power spectra and we conclude in Section 6. Throughout we will assume a Λ CDM cosmological model consistent with the latest *Planck* results [3, 9] and quote distances in comoving h^{-1} Mpc.

2 N-body simulations

To validate our model and further investigate the impact of non-linearity, bias and redshift-space distortions on primordial features we have run a number of N-body simulations. For each of several models we generated 6 realizations of Gaussian initial conditions at $z = 9$ using 2nd order Lagrangian perturbation theory and employed the FASTPM code [10] to evolve 4096^3 particles in a $2.5 h^{-1}$ Gpc box with a $(3 \times 4096)^3$ force grid over 40 time steps linearly spaced in the scale factor, a , down to $z = 0.5$. With 40 steps, which improves the convergence at higher k , the code behaves very much as a traditional particle mesh code.

Each model employed the same background cosmology, of the Λ CDM family and consistent with the latest constraints from PLANCK [9]. Halo catalogs and 5 per cent of the dark matter particles were output at $z = 2, 1$ and 0.5 . The density power spectra in real and redshift space and the real-space velocity spectra were computed using the NBODYKIT software [11]. Fourier transforms were done on a 4096^3 mesh. We bin the spectra in linear k bins of width $\Delta k = 0.005 h \text{ Mpc}^{-1}$ starting at $k_{\min} = 0.005 h \text{ Mpc}^{-1}$. We compute power spectrum “wedges”, $P(k, \mu)$, in 5 equal width μ bins centered at $\mu = 0.1, 0.3, 0.5, 0.7$ and 0.9 , as well as power spectrum multipoles, $P_\ell(k)$ for $\ell = 0, 2$ and 4 . We do not remove shot noise from any of our

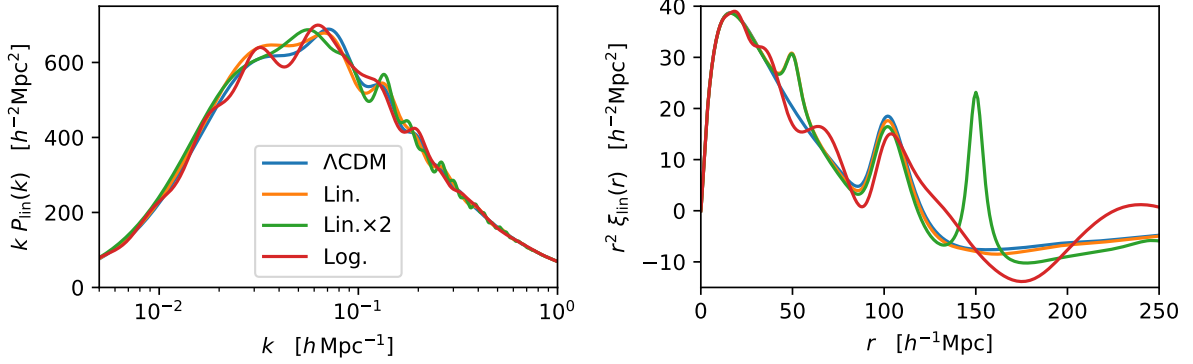


Figure 1. The linear theory power spectra (left) and correlation functions (right) for our fiducial Λ CDM model and models with primordial features superposed. The “Lin.” model has sinusoidal oscillations linear in k (Eq. 3.1), the “Lin. $\times 2$ ” model has sinusoidal oscillations linear in k with two frequencies ($\omega_1 = 50 h^{-1} \text{Mpc}$ and $\omega_2 = 150 h^{-1} \text{Mpc}$) and the “Log.” model has sinusoidal oscillations in $\ln k$ (Eq. 3.2). See text for further details.

spectra, but rather include such contributions in our models. We present the average of the $P(k, \mu)$ with the line of sight taken along each of the cardinal directions of the box.

We have chosen to focus on two, mass limited halo samples, with densities of $10^{-3} h^3 \text{Mpc}^{-3}$ and $10^{-4} h^3 \text{Mpc}^{-3}$. These are characteristic of densities achieved by surveys such as DESI [12], MegaMapper [13] or MSE [14], though significantly sparser than one might expect from future 21 cm experiments [15]. We will highlight the results from the denser sample — which we will call the fiducial sample throughout — since it is less noisy, but the results are qualitatively similar for the lower density sample.

3 Feature models

We will consider two broad classes of “features” in the linear theory power spectrum. The first will arise in the very early Universe (primordial features), for example when the perturbations were originally generated by inflation. The second will be imprinted after inflation but at much earlier times than the epoch of the observations. Let us take each in turn.

3.1 Primordial features

We investigate several phenomenological models of primordial features, chosen to illustrate various issues and highlight results, rather than models based on fundamental physics calculations. Specifically we follow the recent literature in considering two types of oscillations that are superposed upon the linear theory power spectrum computed for Λ CDM,

$$P_{\text{lin}}(k) = P_{\Lambda\text{CDM}}(k) \left\{ 1 + A \sin(\omega k) \exp\left[-\frac{(kr_d)^2}{2}\right] \right\} \quad (\text{linear}) \quad (3.1)$$

and

$$P_{\text{log}}(k) = P_{\Lambda\text{CDM}}(k) \left\{ 1 + A \sin\left(\omega \ln \frac{k}{k_*}\right) \exp\left[-\frac{(kr_d)^2}{2}\right] \right\} \quad (\text{logarithmic}) \quad (3.2)$$

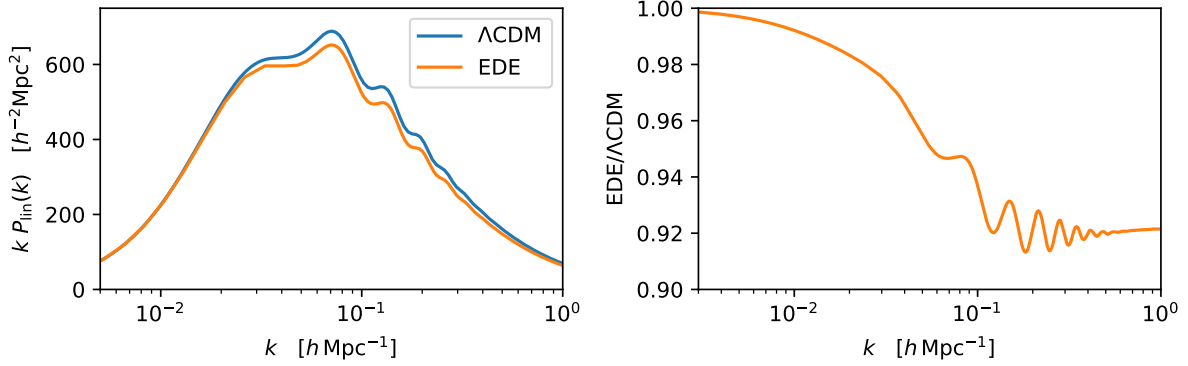


Figure 2. The linear theory power spectra (left) and their ratio (right) for our fiducial Λ CDM model and models with features induced by a period of early dark energy (EDE) at $z \simeq 10^4$. See text for further details.

with $A = 0.05$, $k_* = 0.05 h \text{ Mpc}^{-1}$ and $r_d = 2.5 h^{-1} \text{ Mpc}$. The first class of models have oscillations linear in k , often termed “sharp features”, and tend to arise if the inflaton temporarily departs from its slow roll (attractor) evolution. The second class, with oscillations in $\ln k$, are also termed “resonant features” [5]. Compared to earlier work we have chosen a particular phase for the linear oscillations so that the modification tends to zero at low k and damped the models at high k with a Gaussian. The high k damping more closely reproduces the models based on features in the inflationary potential which tend to produce band-limited oscillations (e.g. refs. [16]), and also ensures that our simulations are properly, numerically resolving the features. While models with 5 per cent oscillations such as these are observationally disfavored [7, 8], using larger amplitude oscillations provides higher signal to noise in our simulations and a more stringent test of the modeling formalism. For the linear model we choose $\omega = 50 h^{-1} \text{ Mpc}$, to emphasize non-linear evolution of the feature compared to the BAO, while for the logarithmic model we take $\omega = 10$, which ensures we resolve the oscillations well with our $2.5 h^{-1} \text{ Gpc}$ box. The linear theory power spectra and correlation functions, extrapolated to $z = 0$, are shown in Fig. 1.

One of the advantages of the linear model is that it can be thought of as a single mode in a Fourier decomposition of a more general class of features. Since all of our models are built upon a Λ CDM template, a second feature (due to baryon acoustic oscillations in the recombination-era Universe [2]) is always present. However, in order to gauge how well we can model non-linear evolution, bias and redshift-space distortions in the presence of multiple frequencies we also generate a linear model with two sine modes of frequencies $\omega_1 = 50 h^{-1} \text{ Mpc}$ and $\omega_2 = 150 h^{-1} \text{ Mpc}$ (Fig. 1). Each mode has the same damping and amplitude as for the “linear” model above.

3.2 Induced features

As a second class of features we consider changes to the matter power spectrum that arise due to non-standard expansion histories. Since the growth of structure is damped by Hubble expansion, long periods where unclustered species dominate the expansion lead to suppression of large-scale structure that can be detected by comparing early- and late-time measures of the

fluctuation amplitude. A precise measurement of the power spectrum shape can also be used to place constraints on (or detect) short-term deviations from matter or radiation domination, since such periods will change the shape of the power spectrum due to differential growth of modes. Recently this reasoning was used to place constraints on early dark energy (EDE) models which contribute to the expansion near recombination [17–20]. The point is more general however, and an accurate measurement of the power spectrum constrains deviations in the expansion history over a broad range of redshifts¹.

As an exploration of these effects we consider scalar-field based models of EDE as in ref. [17], where the impact of EDE is localized to times significantly before those probed observationally. In fact we use the modification of CLASS [21] by the authors of ref. [17] and consider a model where the contribution from EDE peaks at $z \simeq 10^4$ with peak fractional contribution (to ρ) of 10 per cent.

The linear theory power spectrum for this model is compared to our fiducial Λ CDM model in Fig. 2, with the right panel showing the ratio to better highlight the change in shape induced by the non-standard expansion history. The position and amplitude of the feature in the right panel of Fig. 2 are set primarily by the redshift at which the EDE becomes non-negligible and the fraction of the energy density in dark energy (respectively).

4 Peturbative model

4.1 Overview of Previous Work

The effect of non-linearities and long-wavelength modes (IR-resummation) on oscillatory features in the power spectrum has long been studied in the context of BAO. A large body of work shows that these features can be accurately modeled in Lagrangian [22–33] and Eulerian [34–43] perturbation theory.

A perturbative analysis of features based on the Eulerian framework has been done recently [8, 44] (see also ref. [45]), in which the authors studied the effects of long wavelength modes on the primordial features of types given by Eqs (3.1) and (3.2). An important finding of these studies is that higher-loop corrections give rise to $\mathcal{O}(1)$ modifications to the features for a wide range of parameters and wavenumbers of interest. This leads one to consider resumming these $\mathcal{O}(1)$ contributions, arising from the large displacements, as is done in the case of BAO (see above).

For a general, oscillatory power spectrum component, refs. [8, 44] show that the long modes' effect on the one-loop contribution can be computed as

$$P_{1\text{-loop}}^w(k) = \frac{1}{2} \int^\Lambda \frac{d^3 p}{(2\pi)^3} \frac{(\mathbf{p} \cdot \mathbf{k})^2}{p^4} P^{\text{nw}}(k) \left[P^w(|\mathbf{k} + \mathbf{p}|) + P^w(|\mathbf{k} - \mathbf{p}|) - 2P^w(k) \right], \quad (4.1)$$

where Λ is a cut-off scale such that $p < \Lambda \sim k$. Taylor expanding the first two components in the brackets of integrand in q and formally integrating gives a one-loop contributions of the form

$$P_{1\text{-loop},X}^w(k) = -\frac{1}{2} k^2 \Sigma_X^2 P^w(k), \quad (4.2)$$

¹While we do not consider it here, features can also be introduced by interactions between or among particle species

where Σ_X is the effective displacement dispersion at a point and X labels either the linear, or logarithmic shapes given in Eqs (3.1) and (3.2). The dispersion can be well approximated by

$$\Sigma_X^2 = \frac{1}{3\pi^2} \int_0^\Lambda dp [1 - j_0(\omega_X p) + 2j_2(\omega_X p)] P^{\text{nw}}(p), \quad (4.3)$$

where for linear² shapes (Eq. (3.1)) we have $\omega_X = \omega_{\text{lin}}$, while for logarithmic shapes we have $\omega_X = \omega_{\text{log}}/k$. The latter makes a further approximation that, due to the shape of P^{nw} , the Σ_{log} integral has most of its contributions from the $p \ll k$ part of the integral. In the case of linear oscillations the above expression corresponds to the results obtained in BAO studies and their IR-resummations.

Following the results of ref. [44], the total non-linear matter power spectrum at one-loop can be obtained as

$$P_{1\text{-loop},X}(k) = P^{\text{nw}}(k)_L + \left(1 + \frac{1}{2}k^2\Sigma_X^2\right) e^{-\frac{1}{2}k^2\Sigma_X^2} P^{\text{w}}(k)_L + P_{1\text{-loop}}^{\text{nw}} \left[P_L^{\text{nw}} + e^{-\frac{1}{2}k^2\Sigma_X^2} P_L^{\text{w}} \right] (k). \quad (4.4)$$

This expression can readily be extended to the power spectrum for biased tracers, since the above IR-resummation procedure remains unchanged. Moreover we see that if more than a single distinct feature is present in the power spectrum (as is the case if one studies e.g. BAO and some other feature), the above expression simply obtains additive P^{w} contributions, given that, to a very good approximation, we can neglect the cross-correlation contributions of different wiggle components (e.g. $P_{\text{lin}}^{\text{w}} \times P_{\text{BAO}}^{\text{w}}$). For further details on these results we refer a reader to refs [8, 44]. In what follows we shall show how the IR resummation is naturally handled in LPT, and how this leads to a different way of obtaining an Eulerian resummation procedure.

4.2 Lagrangian IR Resummation and Connection to Earlier Approaches

In contrast to the above, within the Lagrangian framework (LPT) IR resummation can be naturally incorporated by exponentiating long-wavelength displacements [23, 28, 32]. Within ΛCDM this is nearly equivalent to simply exponentiating the linear displacements, such that the matter power spectrum for example is given by

$$P_m = \int d^3\mathbf{q} e^{i\mathbf{k}\cdot\mathbf{q} - \frac{1}{2}k_i k_j A_{ij}^{\text{lin}}} \left\{ 1 - \frac{1}{2}k_i k_j A_{ij}^{\text{loop}} + \frac{i}{6}k_i k_j k_k W_{ijk} + \dots \right\}, \quad (4.5)$$

where A_{ij} and W_{ijk} are n -point statistics of pairwise displacements $\Delta = \Psi_1 - \Psi_2$ with separation $\mathbf{q} = \mathbf{q}_1 - \mathbf{q}_2$. Within LPT, the Eulerian resummation can be recovered as a saddle-point approximation; briefly, for an input linear power spectrum with smooth and wiggly components $P_{\text{lin}} = P_{\text{nw}} + \Delta P_X$, the latter can be expanded out of the exponent, where its configuration-space

²These derivations always assume the $r_d \rightarrow 0$ limit.

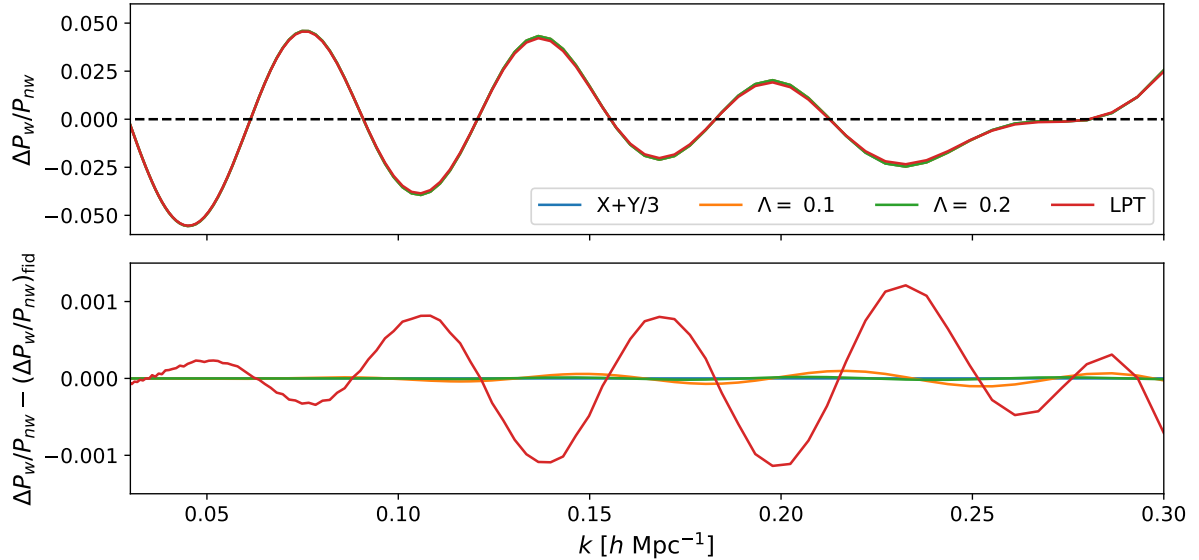


Figure 3. Comparison of the oscillatory components of the real-space power spectrum for our fiducial halo sample at $z = 1$ as predicted by 1-loop EPT and LPT for a range of IR-resummation choices in the Λ CDM cosmology. All choices are in excellent numerical agreement – the EPT schemes are all within 10^{-4} of the total broadband power of each other and differ at the 10^{-3} level with the LPT prediction. The latter number lets us place a minimum theoretical error on predictions for feature amplitude.

feature at some characteristic separation q_X ³ will pick out a nonlinear smoothing

$$e^{-\frac{1}{2}k^2\Sigma_X^2} = \left\langle \exp \left\{ -\frac{1}{2}k_i k_j A_{ij}^{nw,lin}(\mathbf{q}) \right\}_{|\mathbf{q}|=q_X} \right\rangle. \quad (4.7)$$

This recovers the $\Lambda \rightarrow \infty$ limit of Eq. 4.3. The brackets in the above equation refer to the angular average of the exponent in the space of \mathbf{q} 's. Decomposing $A_{ij} = X(q)\delta_{ij} + Y(q)\hat{q}_i\hat{q}_j$ into scalar components X and Y , the most straightforward approach is to take the average to correspond to $X + Y/3$, though we note for example that Eq. 4.3 corresponds to taking $X + Y$. If there are multiple oscillatory components, i.e. a superposition of sinusoidal components as in “Lin.x2” (Fig. 1), then as long as each component is perturbatively small the above argument can be applied independently to determine the saddle-point q_X and damping factor Σ_X^2 of each feature as argued for EPT in the discussion below Eq. 4.4.

Based on the Eulerian and Lagrangian discussions above it may seem like there exists an over-abundance of possible IR resummation schemes. This is not, however, a matter of great concern since it turns out all of these schemes behave quantitatively similarly, at least within

³In general the scale depends upon the first derivative of the argument of the sine. For logarithmic wiggles the Eulerian treatment is equivalent to making the approximation

$$\sin \left(\omega \ln \frac{k}{k_*} \right) \approx \sin \left(\frac{\omega}{k_0} (k - k_0) + \phi_0 \right), \quad (4.6)$$

which at each k picks out the characteristic scale $q_X(k) = \omega/k$. This approximation works increasingly well the larger ω is (see Appendix A).

roughly Λ CDM cosmologies. Figure 3 shows a comparison of these schemes for our fiducial Λ CDM cosmology at $z = 1$, with bias parameters taken from our fiducial halo sample. Taking $\Sigma_X^2 = X + Y/3$ derived from Eq. 4.7 as our baseline (blue curve), we see that the differences between this choice and the conventional EPT dampings with $\Lambda = 0.1, 0.2 \text{ } h\text{Mpc}^{-1}$ are extremely small and at the level of 10^{-4} when compared to the (linear theory) broadband power. This is because much of the numerical difference between the “linear” $e^{-\frac{1}{2}k^2\Sigma_X^2}\Delta P_w$ is ameliorated by correctly accounting for damping effects at one-loop level in Eq. 4.4. On the other hand, the differences between these schemes and a direct LPT calculation in which the linear displacements are fully resummed is larger, though still in excellent numerical agreement, at about the 10^{-3} level. Finally, let us note that while the (Gaussian) statistical error on power spectrum measurements scale as amplitude of the total power, the theory error discussed above scales as the amplitude of the wiggles only; for example, while it is at 10^{-3} of the total power for the a 5% feature (BAO), non-BAO primordial features bounded at the 1% level using BOSS and Planck data by ref. [8], it will be at the 2×10^{-4} level at the same redshift.

From the above comparison, we can conclude that (1) the disagreement between LPT and EPT lets us set a minimum theoretical error on theoretical predictions for feature amplitude at about 0.1% and (2) that the difference between the various Eulerian IR resummation schemes and their predictions for Σ_X^2 are small compared to this theoretical error, such that we can be reasonably cavalier when choosing between them. Indeed, as k approaches the nonlinear scale we should expect that oscillatory signals from beyond-one-loop contributions will become increasingly prominent compared to the amplitude of the linear oscillations, dwarfing the theoretical differences highlighted above in the same way that the scale of the bottom panel of Figure 3 is much smaller than that of the top panel. Given that the one-loop EPT-LPT difference is only a few percent of the wiggle amplitude in Λ CDM—5 percent compare to 0.1 percent—even at the edge of our perturbative reach at $k = 0.2h \text{ Mpc}^{-1}$, the above comparison suggests that searches for primordial features should focus on exploring higher redshifts and volumes.

4.3 Redshift-Space Distortions

Since next-generation galaxy redshift surveys will be the natural hunting ground for primordial features, the focus of this paper is to extend the modeling of primordial features in previous works to redshift space. We use 1-loop Lagrangian and Eulerian perturbation theory (LPT and EPT) described in the previous subsections to model both the real- and redshift-space power spectra of biased tracers (i.e. halos in our context) as described in detail in ref. [46]. The redshift-space power spectrum, $P_s(k, \mu)$, is evaluated as an expansion in the line-of-sight wavenumber, $k_{\parallel} = k\mu$, multiplying n^{th} -order pairwise velocity spectra, such that

$$P_s(k, \mu) = \sum_{n=0}^{\infty} \frac{(ik\mu)^n}{n!} \tilde{\Xi}_{\parallel}^{(n)}(k, \mu). \quad (4.8)$$

The model includes Lagrangian and Eulerian third-order bias expansions along with counter terms and stochastic terms to account for small-scale physics that we do not explicitly model. Our fiducial model includes terms up to second order in the velocity expansion, but employ an ansatz for the third moment which is shown to be highly accurate for Λ CDM-like models [46]. As discussed in ref. [46], while a finite-order expansion in the velocity moments $\tilde{\Xi}$ necessarily omits

feature damping due to bulk velocities that would be included in a “complete” IR resummation scheme, particularly at high μ , we will show that it is nonetheless sufficiently accurate for upcoming galaxy surveys like DESI; however, for completeness we also include comparisons to (1) the Gaussian streaming model and (2) one-loop EPT wherein both bulk displacements and velocities are resummed where appropriate. We set the third order Lagrangian bias to zero since its effects are subdominant for the halos and scales of interest [47, 48].

5 Results

To see how well our perturbative models predict the non-linear evolution and redshift-space distortions in models with primordial or induced features we compare to our N-body results. For each model we fit to the average of the 6 simulations. The fits are done using the model “out of the box”, i.e. without tweaking or adjusting any settings, letting only bias parameters and effective corrections float, and assuming the correct cosmology and linear theory power spectrum. Fixing the cosmology and linear theory power spectrum provides a stringent test, as it does not allow variation in nuisance parameters to “soak up” inaccuracies in the fits.

Figure 4 shows an example of our fits to the real-space halo spectra for the primordial feature models. The real-space spectra are not directly observable (except in projection, which will tend to wash out the features) but serve to show that the model is able to predict the underlying clustering well. We focus on the middle redshift ($z = 1$) and highest number density ($\bar{n} = 10^{-3} h^3 \text{Mpc}^{-3}$) sample since this has the smallest error bars. The agreement between both models and N-body data is excellent over the entire range of quasi-linear scales and into the regime where shot-noise begins to dominate the spectra. While not shown, we have checked that the more biased sample and other redshift slices show similar levels of agreement.

In addition to the real-space power spectrum we have also measured the first two, real-space pairwise velocity moments of our halo samples and compared them to perturbation theory. These velocity statistics inform the angular structure of the redshift-space power spectrum (which we expect will eventually provide our tightest observational constraints on features) in addition to being well-defined observables in their own right, and extracting them individually gives us a closer look at oscillatory features that only become prominent at high μ . Figure 5 shows our best-fit LPT and EPT models for the model with two linear oscillations (Lin. $\times 2$) with broadband shapes subtracted to isolate the oscillatory components⁴. Much as in Λ CDM models [46] there is excellent agreement between LPT and EPT for the real-space power spectrum (P), and the pairwise velocity (v), while EPT tends to slightly underpredict the damping for the second moment (σ_ℓ), especially as the one-loop oscillations become prominent at $k > 0.1 h, \text{Mpc}^{-1}$. These differences are, however, small and the models predict almost identical power spectrum wedges. Nonetheless, they are helpful in informing our theoretical error budget when searching for oscillations close to the line-of-sight.

As Figs. 4 and 5 make clear the Eulerian and Lagrangian descriptions provide almost identical performance over the range of scales where we expect perturbation theory to be valid. We find

⁴In this and other plots of the nonlinear oscillation signal below, we remove broadband differences by fitting a quartic polynomial in k to the differences between plotted curves.

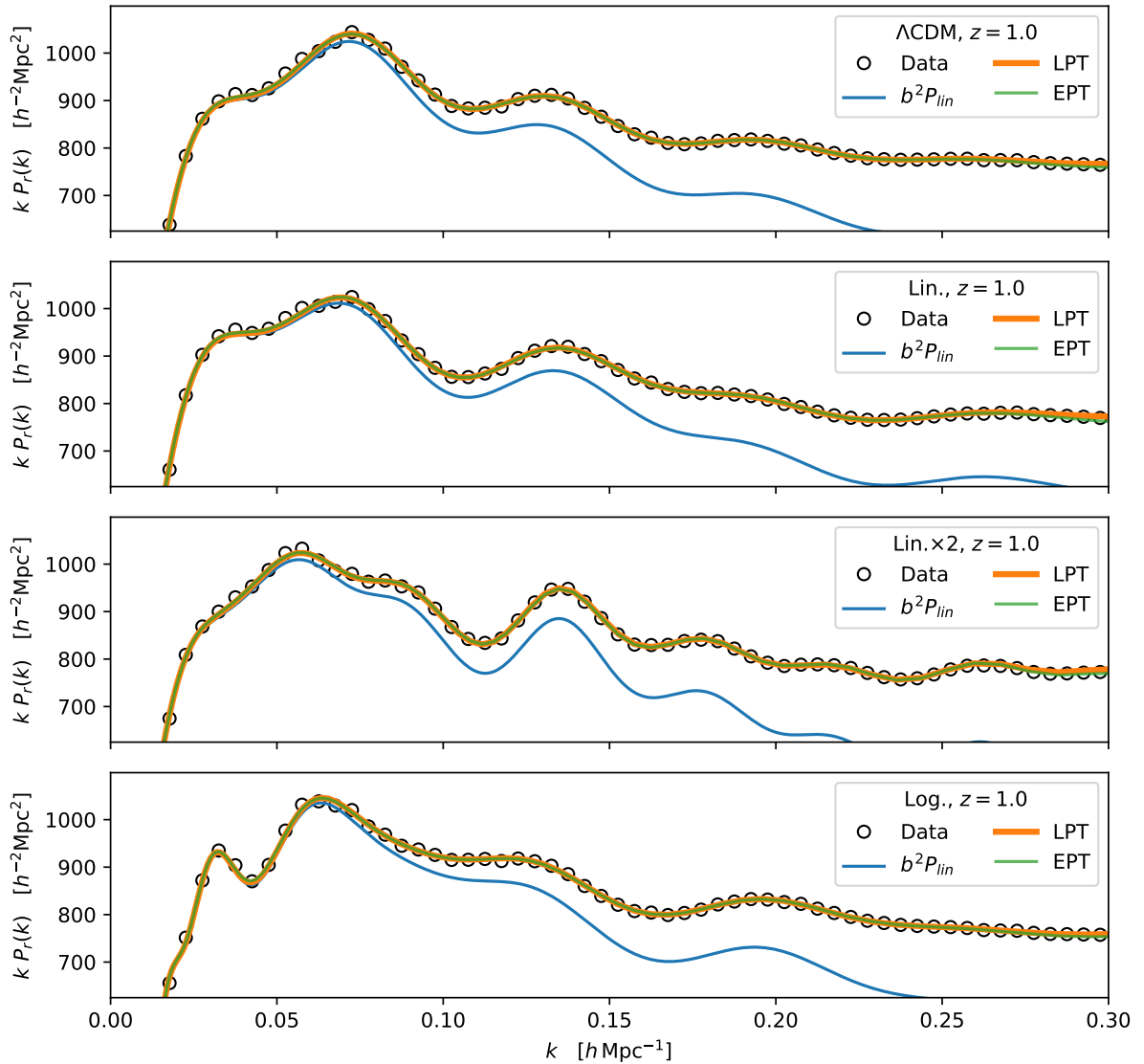


Figure 4. The real-space, halo power spectra from our simulations at $z = 1$ and model fits. We show results for the $\bar{n} = 10^{-3} h^3 \text{Mpc}^{-3}$ sample, since it has lower shot noise, but results for the sparser sample are qualitatively similar. The open, black circles show the average of $P(k)$ over the 4 boxes. The orange and green lines (which are almost on top of each other) show the best-fit LPT and EPT models while the blue line shows linear theory with the same large-scale bias as the EPT models.

this persists even for the redshift-space spectra, and so to avoid clutter we shall show only the Lagrangian model in the following figures.

Figure 6 compares the theory prediction (LPT moment expansion) and N-body data for the anisotropic power spectrum wedges $P(k, \mu)$ in redshift space. The theory and data are in excellent agreement over a large range of scales and LOS angles μ , though we note that the shot noise $\sim \bar{n}^{-1}$ plays an increasingly dominant role at the highest k 's shown. We focus on the redshift-space wedges, which are independent in linear theory, but have checked that the theory returns

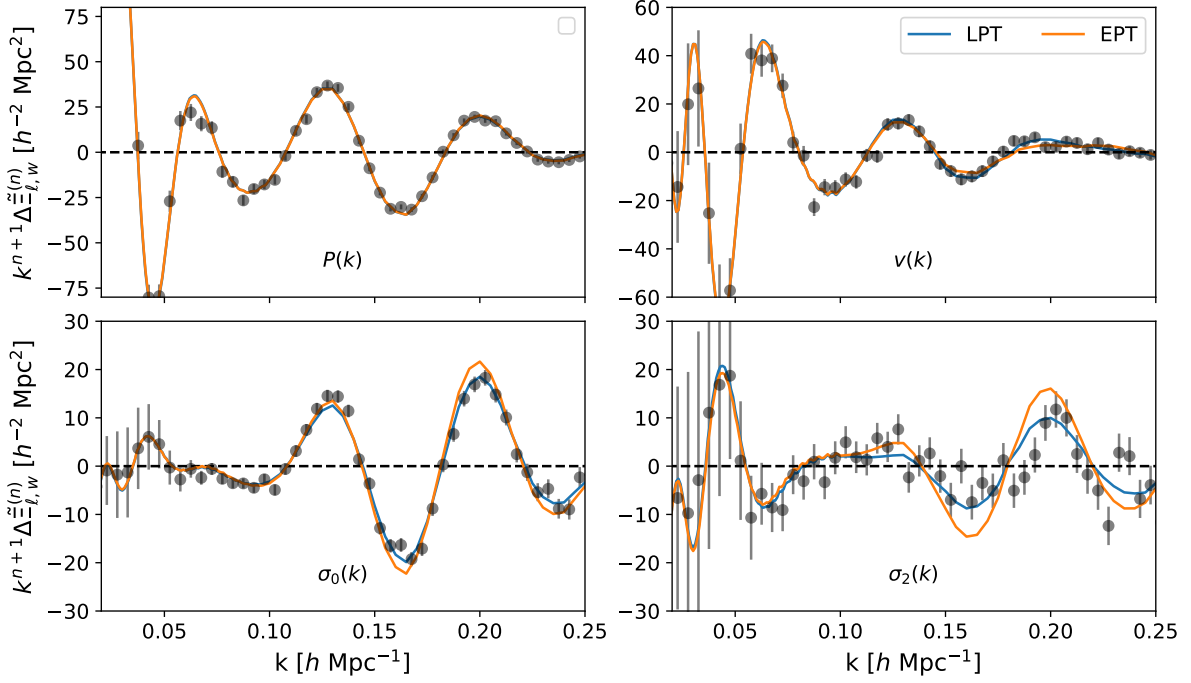


Figure 5. Broadband-subtracted pairwise-velocity moments in real space for our fiducial halo sample with the “Lin. $\times 2$ ” linear power spectrum compared to predictions from LPT and EPT. As in basic Λ CDM models, there is excellent quantitative agreement between LPT and EPT in the zeroth and first moments, while in the second moment EPT slightly underpredicts the damping of 1-loop wiggles prominent at higher k .

an equivalently good fit to the smooth and oscillatory components of the multipoles.

As an additional check on possible theory differences, Fig. 7 shows the predictions for the oscillatory components of $P_\ell(k)$ (i.e. with the broadband subtracted) for our fiducial halo sample using our LPT moment expansion model, Gaussian streaming model and resummed Eulerian perturbation theory. Despite the Lagrangian and Eulerian models being fit separately to the wedges, i.e. $P(k, \mu)$ data, all three models are in excellent agreement with each other and the N-body data for the multipoles, $P_\ell(k)$. The agreement is particularly impressive in comparison to the scatter in the N-body data, which are themselves tighter than expected for upcoming surveys with a total simulated volume of $> 90 h^{-3} \text{Gpc}^3$. In order to demonstrate their equivalence at low k , we have matched the counterterms between the moment expansion and Gaussian streaming model predictions (Appendix B), but note that at the highest k ’s shown the GSM predictions for the quadrupole are in fact in slightly better agreement with the EPT prediction, suggesting that differences there are driven by the incomplete IR resummation of bulk velocities in the moment expansion (see ref. [46] for further discussion).

Finally, Fig. 8 shows similar fits to the model with 10 per cent early dark energy at $z \simeq 10^4$. Again the model provides an excellent fit to the N-body data in both real and redshift space on quasi-linear scales, indicating that these scales can be used to constrain the amount of unclustered dark energy contributing to the expansion when such modes entered the horizon. Future surveys,

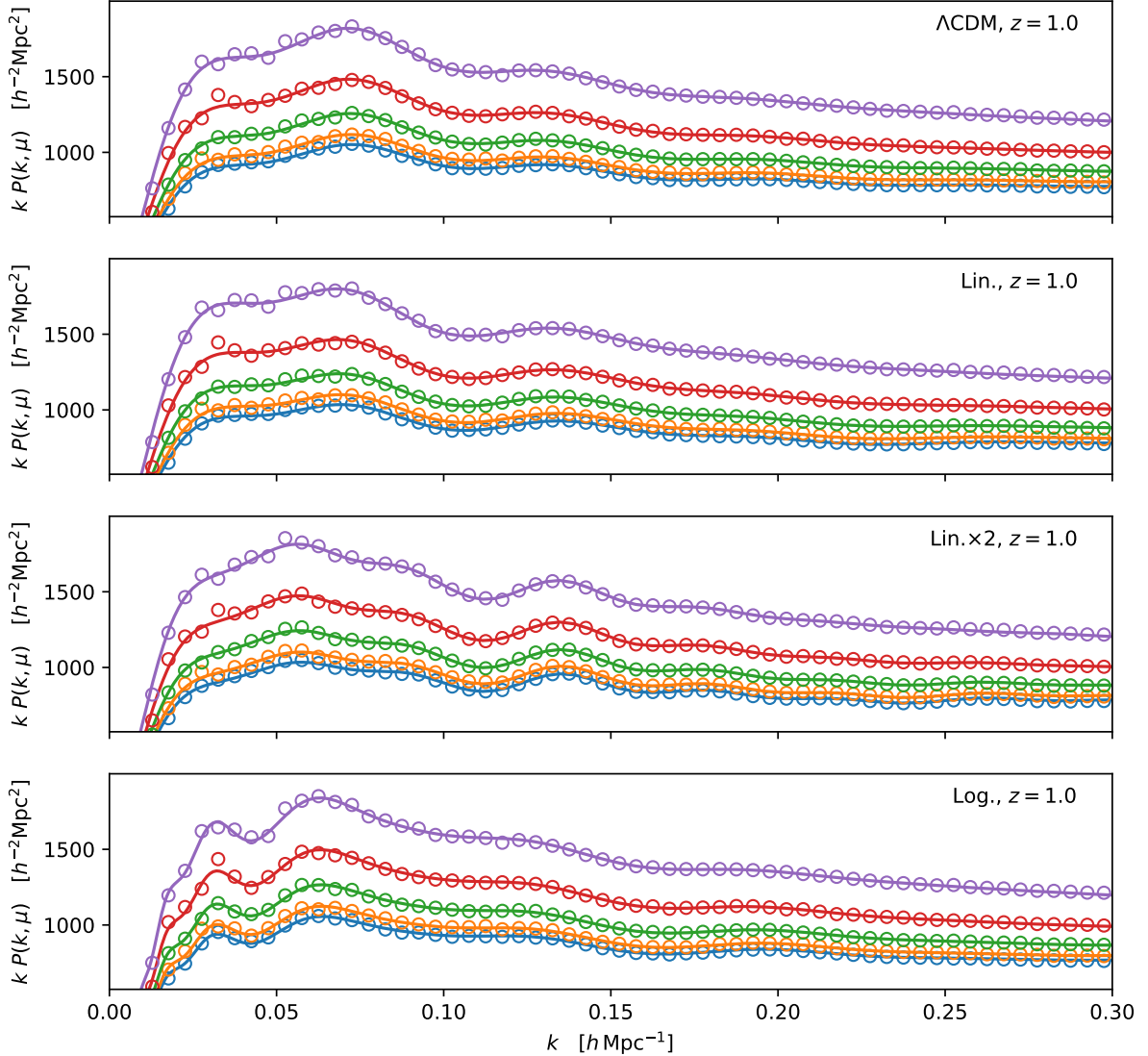


Figure 6. The redshift-space, halo power spectrum wedges from our simulations at $z = 1$ and model fits. We show results for the $\bar{n} = 10^{-3} h^3 \text{ Mpc}^{-3}$ sample, since it has lower shot noise, but results for the sparser sample are qualitatively similar. The open circles show the average of $P(k, \mu)$ for $\mu = 0.1, 0.3, \dots, 0.9$ (colors, bottom to top), the solid lines show the best-fit LPT model.

probing large volumes at high redshift, should be able to constrain the expansion history via its effect on growth over a broad range of cosmic history.

6 Conclusions

We have investigated how well 1-loop perturbation theory, both Eulerian and Lagrangian, can model the redshift-space power spectra of biased tracers such as dark matter halos in models with either primordial or induced features. By comparing the models of ref. [46] to clustering statistics

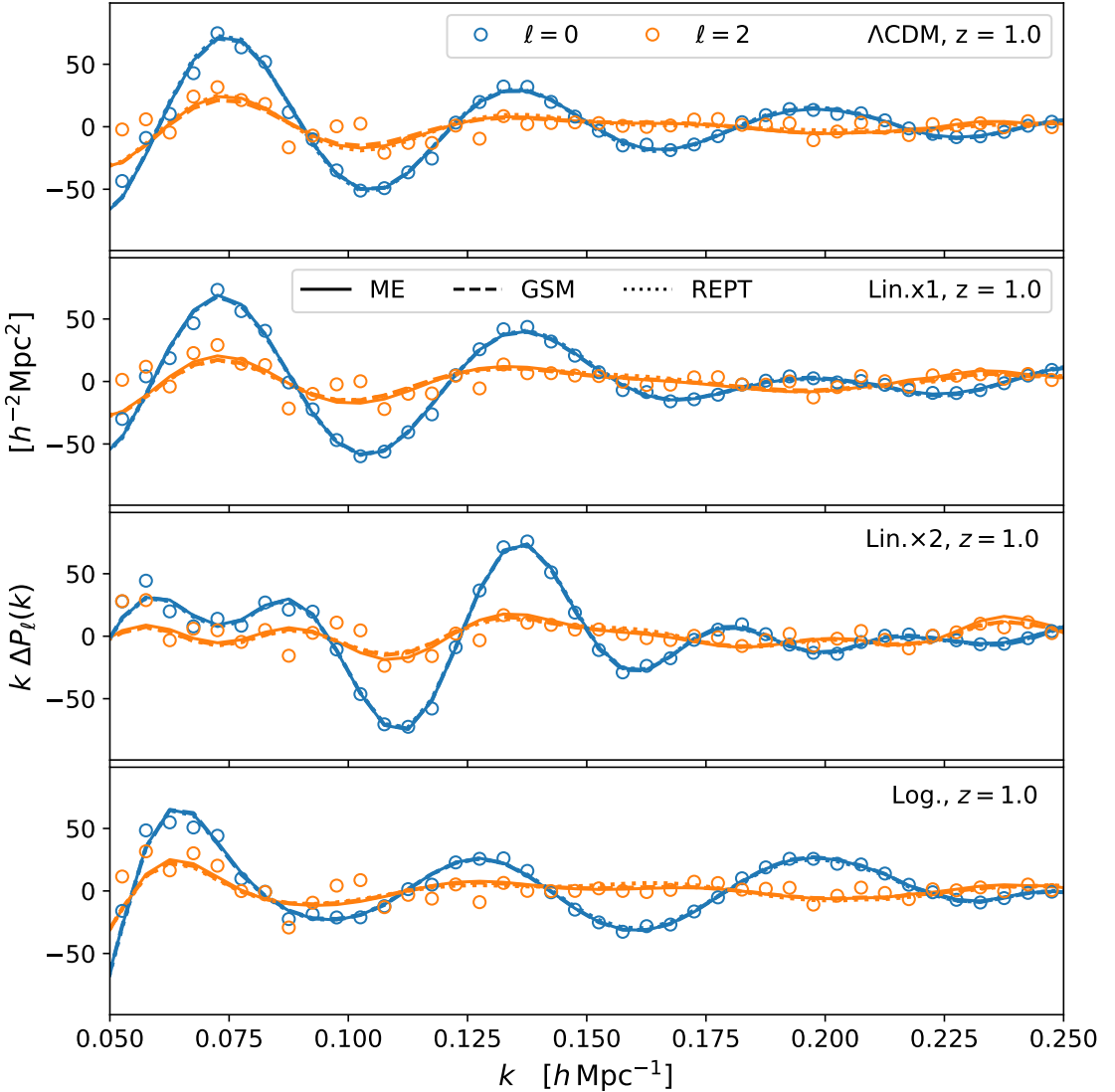


Figure 7. Predictions using the LPT moment expansion, Gaussian streaming model and IR-resummed EPT (REPT) for the oscillatory components of the redshift-space power spectrum monopole and quadrupole at $z = 1$ for the $\bar{n} = 10^{-3} h^3 \text{Mpc}^{-3}$ sample. The LPT and REPT models are in excellent agreement, especially compared to the scatter of the N-body data to which they were independently fit.

measured from a series of large N-body simulations, we have shown that bias, non-linear evolution and redshift-space distortions can all be accurately accounted for by existing perturbative models with no need for any tuning or modification. This is the first demonstration that such perturbative models can fit the redshift-space clustering of biased tracers in such theories to per cent level precision on quasi-linear scales.

We compare three primordial feature models (Fig. 1) and one model with an “induced” feature imprinted by an epoch of early dark energy (Fig. 2). We investigated two different schemes for

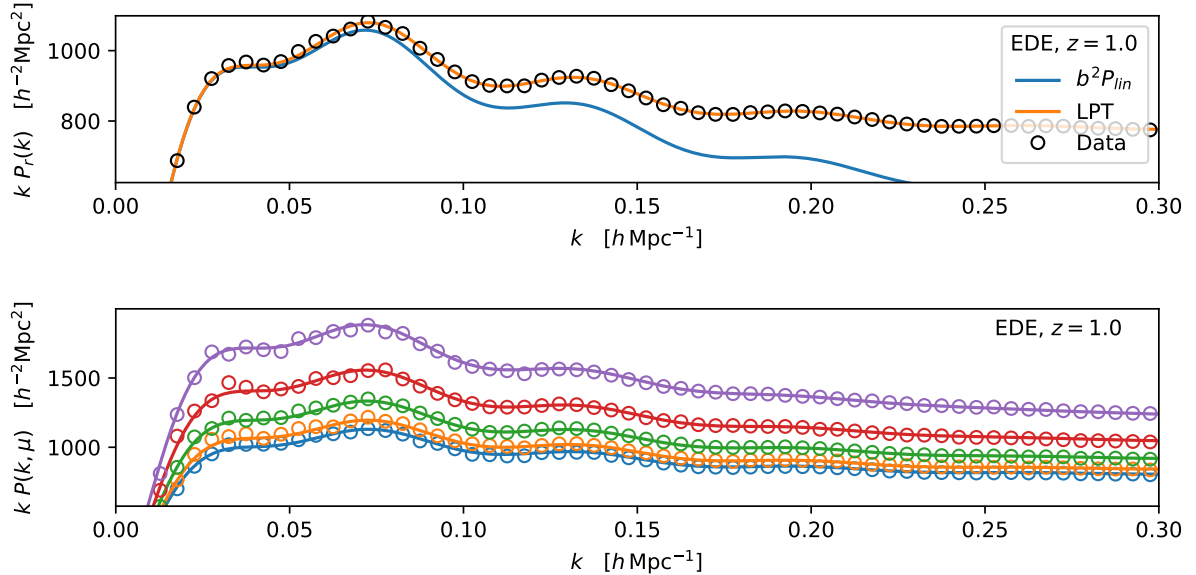


Figure 8. As for Figs. 4 and 6 but for the model with an “induced feature” (see text and Fig. 2).

modeling the dynamics (Eulerian and Lagrangian), several different IR resummation schemes, and different methods for including redshift-space distortions (a moment expansion and a cumulant expansion: the Gaussian Streaming Model). In all cases we find excellent agreement between the different theories and the N-body simulations. Figure 3 shows that different methods of performing IR resummation give extremely similar predictions for the power spectrum. Figures 4 and 5 show that both LPT and EPT predict the real-space density and velocity statistics measured in our N-body simulations well to $k \simeq 0.25 h \text{ Mpc}^{-1}$. With these ingredients, Fig. 6 shows that the moment expansion accurately describes the redshift-space, power spectrum wedges, $P(k, \mu)$ with Fig. 7 highlighting the agreement on the oscillatory features in the multipole moments for both the moment expansion and a cumulant expansion. Figure 8 shows the same excellent agreement for features induced by changes in the expansion history at high redshift, rather than imprinted upon the primordial power spectrum.

This extensive set of comparisons and tests imply that current perturbative models are up to the task of constraining models with features given suitably accurate redshift-space clustering data. Future surveys, capable of operating over large volumes at high redshift — shifting the non-linear scale to higher k and the fundamental mode to lower k — would be ideal in providing such constraints. We intend to return to the detectability of these features by different surveys [45], and the impact of degeneracies, in a future paper. However, it is clear that future surveys that probe large volumes at high redshift should be able to constrain both primordial features and the expansion history over a broad range of cosmic history (via its effect on growth).

Acknowledgments

We would like to thank Emanuele Castorina, Sergey Sibiryakov, and Marko Simonović for many useful discussions. We also thank the authors of ref. [17] for making public their modification of the CLASS Boltzmann code including early dark energy. S.C. is supported by the National Science Foundation Graduate Research Fellowship (Grant No. DGE 1106400) and by the UC Berkeley Theoretical Astrophysics Center Astronomy and Astrophysics Graduate Fellowship. M.W. is supported by the U.S. Department of Energy and the NSF. This research has made use of NASA's Astrophysics Data System and the arXiv preprint server. This research used resources of the National Energy Research Scientific Computing Center (NERSC), a U.S. Department of Energy Office of Science User Facility operated under Contract No. DE-AC02-05CH11231.

A Saddle-Point Approximation for Nonlinear Dispersions

In this appendix we expand upon the argument for selecting scale $q = \omega/k$ in the logarithmic case, and show it follows as a special case of a more general expression in the large ω limit. Suppose we have

$$\Delta P_X(k) = P_{\Lambda\text{CDM}}(k) \sin(\omega\phi(k)) \quad (\text{A.1})$$

where ω is a constant tunable parameter such that $\omega\phi(k)$ is the (nonlinear) phase of the oscillating feature. We are interested in applying the saddle-point result for linear oscillations to this case.

Around some wavenumber $k = k_0$ of interest, we can Taylor-expand the phase as

$$\omega\phi(k) \simeq \omega \left(\phi_0 + \phi'_0(k - k_0) + \frac{1}{2}\phi''_0(k - k_0)^2 + \dots \right) \quad (\text{A.2})$$

where primes indicate derivatives with respect to k . Roughly, the linear approximation $\phi_L = \phi_0 + \phi'_0(k - k_0)$ will be good provided that $|k - k_0| < |\phi'_0/\phi''_0|$ independently of ω . This also defines the window within which to a good approximation $d\phi/dk \approx \phi'_0$.

However, unless $\phi(k)$ is linear, this window is not guaranteed to cover all interesting k . To restrict our calculation to the interval around k_0 where the linear approximation is valid, let us multiply by a function $W(k, k_0)$ with support in the interval and which falls to zero away from k_0 with characteristic width $\sigma_k = |\phi'_0/\phi''_0|$. Then we can approximate $W(k, k_0) \sin(\omega\phi(k))$ as $W(k, k_0) \sin(\omega\phi_L(k))$ everywhere. In addition, for the saddle-point approximation to work we also require that the Fourier-transformed feature be sharply localized at some scale, which will be equal to $q_X = |\omega\phi'_0|$ in our case. This condition is controlled by ω , since the number of cycles within our interval is $N_{\text{cyc}} = (2\pi)^{-1}|\omega\phi'^2_0/\phi''_0|$; for a given $\phi(k)$ the bigger ω is the better.

Following the above we have that the “windowed” feature $W(k, k_0) \Delta P_X(k)$ receives a damping factor well-approximated by $\Sigma^2(q_X = |\omega\phi'_0|)$. By the same logic we can fill out the oscillatory signal by sequence of windows $W(k, k_i)$ each with width $\sim |\phi'_i/\phi''_i|$ such that $\sum_i W(k, k_i) = 1$ at all k . Then, at any k we have that the damping is given by $\Sigma^2(q_X = |\omega\phi'_i|)$, which will to a very good approximation be equal to $\phi'(k)$ from our previous arguments.

Let us apply this argument for the logarithmic features as an example. Setting $\phi(k) = \ln(k/k_*)$, we see that the width is set by $\sigma_k \sim k$ and that the requirement $N_{\text{cyc}} \gg 1$ is equivalent to $\omega \gg 2\pi$. This limit is met by our fiducial $\omega = 10$ and by the frequencies explored in the BOSS

data in ref. [8], who also set a related criterion for the sharpness of primordial features. Note that the fact that the corresponding ω 's are large also implies that the approximation $\phi'(k) \approx \phi'_i$ is a good one, with corrections of order ω^{-1} for fixed N_{cyc} .

B GSM vs. moment expansion

Beyond the moment expansion, the velocity statistics underlying redshift-space distortions can also be expanded via cumulant expansions to yield a variety of so-called streaming models [49]. A popular example is the Gaussian streaming model (GSM) [50, 51], which derives from the cumulant expansion in (real) configuration space at second order. A particular strength of the GSM is its ability to accurately capture the nonlinear smoothing of the BAO feature in redshift space, which can be roughly attributed to the responsible bulk displacements truncating at second order in the configuration-space cumulants [46].

Recently [46], we argued that percent-level modeling of the redshift-space power spectrum requires including the third moment, or at least approximating its effect via a counterterm ansatz. Naively, this would rule out using the GSM for full-shape RSD analyses at intermediate (but perturbative scales); however, a proper accounting of the counterterms in the second moment shows that its quadrupole requires a counterterm degenerate with the above ansatz. Specifically, splitting the two-point function into contributions from large-scale bias and effective corrections as in Eq. 5.1 of ref. [46] and comparing with expressions for the velocity moments in LPT (Eqs. 4.11–15) one sees that the complete set of counterterms for the power spectrum can be obtained within the GSM by setting

$$\alpha_P = \alpha_0, \quad \alpha_v = \alpha_2 - \frac{1}{18}\alpha_4, \quad \alpha_\sigma^{(2)} = -\frac{2}{9}\alpha_4, \quad (\text{B.1})$$

where $\alpha_\sigma^{(2)}$ is the counterterm to the quadrupole of $\sigma_{12}^2(\mathbf{k})$ multiplying the Zeldovich power spectrum $P_{\text{Zel}}(k)$. This implies that the Fourier-transformed GSM can adequately model the redshift-space power spectrum while also accurately capturing nonlinear smoothing of power spectrum features.

References

- [1] J. A. Peacock, *Cosmological Physics*. Jan., 1999.
- [2] S. Dodelson, *Modern cosmology*. 2003.
- [3] Planck Collaboration, Y. Akrami, F. Arroja, M. Ashdown, J. Aumont, C. Baccigalupi, M. Ballardini, A. J. Banday, R. B. Barreiro, N. Bartolo, S. Basak, R. Battye, K. Benabed, J. P. Bernard, M. Bersanelli, P. Bielewicz, J. J. Bock, J. R. Bond, J. Borrill, F. R. Bouchet, F. Boulanger, M. Bucher, C. Burigana, R. C. Butler, E. Calabrese, J. F. Cardoso, J. Carron, B. Casaponsa, A. Challinor, H. C. Chiang, L. P. L. Colombo, C. Combet, D. Contreras, B. P. Crill, F. Cuttaia, P. de Bernardis, G. de Zotti, J. Delabrouille, J. M. Delouis, F. X. Désert, E. Di Valentino, C. Dickinson, J. M. Diego, S. Donzelli, O. Doré, M. Douspis, A. Ducout, X. Dupac, G. Efstathiou, F. Elsner, T. A. Enßlin, H. K. Eriksen, E. Falgarone, Y. Fantaye, J. Fergusson, R. Fernandez-Cobos, F. Finelli, F. Forastieri, M. Frailis, E. Franceschi, A. Frolov, S. Galeotta, S. Galli, K. Ganga, R. T. Génova-Santos, M. Gerbino, T. Ghosh, J. González-Nuevo, K. M. Górski, S. Gratton, A. Gruppuso, J. E. Gudmundsson, J. Hamann, W. Handley, F. K. Hansen, G. Helou,

D. Herranz, E. Hivon, Z. Huang, A. H. Jaffe, W. C. Jones, A. Karakci, E. Keihänen, R. Keskitalo, K. Kiiveri, J. Kim, T. S. Kisner, L. Knox, N. Krachmalnicoff, M. Kunz, H. Kurki-Suonio, G. Lagache, J. M. Lamarre, M. Langer, A. Lasenby, M. Lattanzi, C. R. Lawrence, M. Le Jeune, J. P. Leahy, J. Lesgourgues, F. Levrier, A. Lewis, M. Liguori, P. B. Lilje, M. Lilley, V. Lindholm, M. López-Caniego, P. M. Lubin, Y. Z. Ma, J. F. Macías-Pérez, G. Maggio, D. Maino, N. Mandolesi, A. Mangilli, A. Marcos-Caballero, M. Maris, P. G. Martin, E. Martínez-González, S. Matarrese, N. Mauri, J. D. McEwen, P. D. Meerburg, P. R. Meinhold, A. Melchiorri, A. Mennella, M. Migliaccio, M. Millea, S. Mitra, M. A. Miville-Deschénes, D. Molinari, A. Moneti, L. Montier, G. Morgante, A. Moss, S. Mottet, M. Münchmeyer, P. Natoli, H. U. Nørgaard-Nielsen, C. A. Oxborrow, L. Pagano, D. Paoletti, B. Partridge, G. Patanchon, T. J. Pearson, M. Peel, H. V. Peiris, F. Perrotta, V. Pettorino, F. Piacentini, L. Polastri, G. Polenta, J. L. Puget, J. P. Rachén, M. Reinecke, M. Remazeilles, A. Renzi, G. Rocha, C. Rosset, G. Roudier, J. A. Rubiño-Martín, B. Ruiz-Granados, L. Salvati, M. Sandri, M. Savelainen, D. Scott, E. P. S. Shellard, M. Shiraishi, C. Sirignano, G. Sirri, L. D. Spencer, R. Sunyaev, A. S. Suur-Uski, J. A. Tauber, D. Tavagnacco, M. Tenti, L. Terenzi, L. Toffolatti, M. Tomasi, T. Trombetti, J. Valiviita, B. Van Tent, L. Vibert, P. Vielva, F. Villa, N. Vittorio, B. D. Wandelt, I. K. Wehus, M. White, S. D. M. White, A. Zaccari, and A. Zonca, *Planck 2018 results. I. Overview and the cosmological legacy of Planck*, *arXiv e-prints* (July, 2018) arXiv:1807.06205, [[arXiv:1807.06205](https://arxiv.org/abs/1807.06205)].

- [4] J. Chluba, J. Hamann, and S. P. Patil, *Features and new physical scales in primordial observables: Theory and observation*, *International Journal of Modern Physics D* **24** (June, 2015) 1530023, [[arXiv:1505.01834](https://arxiv.org/abs/1505.01834)].
- [5] A. Slosar, X. Chen, C. Dvorkin, D. Meerburg, B. Wallisch, D. Green, and E. Silverstein, *Scratches from the Past: Inflationary Archaeology through Features in the Power Spectrum of Primordial Fluctuations*, *Bulletin of the AAS* **51** (May, 2019) 98, [[arXiv:1903.09883](https://arxiv.org/abs/1903.09883)].
- [6] D. H. Weinberg, M. J. Mortonson, D. J. Eisenstein, C. Hirata, A. G. Riess, and E. Rozo, *Observational probes of cosmic acceleration*, *PhysRep* **530** (Sept., 2013) 87–255, [[arXiv:1201.2434](https://arxiv.org/abs/1201.2434)].
- [7] Planck Collaboration, Y. Akrami, F. Arroja, M. Ashdown, J. Aumont, C. Baccigalupi, M. Ballardini, A. J. Banday, R. B. Barreiro, N. Bartolo, S. Basak, K. Benabed, J. P. Bernard, M. Bersanelli, P. Bielewicz, J. J. Bock, J. R. Bond, J. Borrill, F. R. Bouchet, F. Boulanger, M. Bucher, C. Burigana, R. C. Butler, E. Calabrese, J. F. Cardoso, J. Carron, A. Challinor, H. C. Chiang, L. P. L. Colombo, C. Combet, D. Contreras, B. P. Crill, F. Cuttaia, P. de Bernardis, G. de Zotti, J. Delabrouille, J. M. Delouis, E. Di Valentino, J. M. Diego, S. Donzelli, O. Doré, M. Douspis, A. Ducout, X. Dupac, S. Dusini, G. Efstathiou, F. Elsner, T. A. Enßlin, H. K. Eriksen, Y. Fantaye, J. Fergusson, R. Fernandez-Cobos, F. Finelli, F. Forastieri, M. Frailis, E. Franceschi, A. Frolov, S. Galeotta, S. Galli, K. Ganga, C. Gauthier, R. T. Génova-Santos, M. Gerbino, T. Ghosh, J. González-Nuevo, K. M. Górski, S. Gratton, A. Gruppuso, J. E. Gudmundsson, J. Hamann, W. Handley, F. K. Hansen, D. Herranz, E. Hivon, D. C. Hooper, Z. Huang, A. H. Jaffe, W. C. Jones, E. Keihänen, R. Keskitalo, K. Kiiveri, J. Kim, T. S. Kisner, N. Krachmalnicoff, M. Kunz, H. Kurki-Suonio, G. Lagache, J. M. Lamarre, A. Lasenby, M. Lattanzi, C. R. Lawrence, M. Le Jeune, J. Lesgourgues, F. Levrier, A. Lewis, M. Liguori, P. B. Lilje, V. Lindholm, M. López-Caniego, P. M. Lubin, Y. Z. Ma, J. F. Macías-Pérez, G. Maggio, D. Maino, N. Mandolesi, A. Mangilli, A. Marcos-Caballero, M. Maris, P. G. Martin, E. Martínez-González, S. Matarrese, N. Mauri, J. D. McEwen, P. D. Meerburg, P. R. Meinhold, A. Melchiorri, A. Mennella, M. Migliaccio, S. Mitra, M. A. Miville-Deschénes, D. Molinari, A. Moneti, L. Montier, G. Morgante, A. Moss, M. Münchmeyer, P. Natoli, H. U. Nørgaard-Nielsen, L. Pagano, D. Paoletti, B. Partridge, G. Patanchon, H. V. Peiris, F. Perrotta, V. Pettorino, F. Piacentini, L. Polastri, G. Polenta, J. L. Puget, J. P. Rachén, M. Reinecke, M. Remazeilles, A. Renzi, G. Rocha, C. Rosset, G. Roudier,

J. A. Rubiño-Martín, B. Ruiz-Granados, L. Salvati, M. Sandri, M. Savelainen, D. Scott, E. P. S. Shellard, M. Shiraishi, C. Sirignano, G. Sirri, L. D. Spencer, R. Sunyaev, A. S. Suur-Uski, J. A. Tauber, D. Tavagnacco, M. Tenti, L. Toffolatti, M. Tomasi, T. Trombetti, J. Valiviita, B. Van Tent, P. Vielva, F. Villa, N. Vittorio, B. D. Wandelt, I. K. Wehus, S. D. M. White, A. Zacchei, J. P. Zibin, and A. Zonca, *Planck 2018 results. X. Constraints on inflation*, arXiv e-prints (July, 2018) arXiv:1807.06211, [[arXiv:1807.06211](https://arxiv.org/abs/1807.06211)].

[8] F. Beutler, M. Biagetti, D. Green, A. Slosar, and B. Wallisch, *Primordial features from linear to nonlinear scales*, *Physical Review Research* **1** (Dec., 2019) 033209, [[arXiv:1906.08758](https://arxiv.org/abs/1906.08758)].

[9] Planck Collaboration, N. Aghanim, Y. Akrami, M. Ashdown, J. Aumont, C. Baccigalupi, M. Ballardini, A. J. Banday, R. B. Barreiro, N. Bartolo, S. Basak, R. Battye, K. Benabed, J. P. Bernard, M. Bersanelli, P. Bielewicz, J. J. Bock, J. R. Bond, J. Borrill, F. R. Bouchet, F. Boulanger, M. Bucher, C. Burigana, R. C. Butler, E. Calabrese, J. F. Cardoso, J. Carron, A. Challinor, H. C. Chiang, J. Chluba, L. P. L. Colombo, C. Combet, D. Contreras, B. P. Crill, F. Cuttaia, P. de Bernardis, G. de Zotti, J. Delabrouille, J. M. Delouis, E. Di Valentino, J. M. Diego, O. Doré, M. Douspis, A. Ducout, X. Dupac, S. Dusini, G. Efstathiou, F. Elsner, T. A. Enßlin, H. K. Eriksen, Y. Fantaye, M. Farhang, J. Fergusson, R. Fernandez-Cobos, F. Finelli, F. Forastieri, M. Frailis, A. A. Fraisse, E. Franceschi, A. Frolov, S. Galeotta, S. Galli, K. Ganga, R. T. Génova-Santos, M. Gerbino, T. Ghosh, J. González-Nuevo, K. M. Górski, S. Gratton, A. Gruppuso, J. E. Gudmundsson, J. Hamann, W. Handley, F. K. Hansen, D. Herranz, S. R. Hildebrandt, E. Hivon, Z. Huang, A. H. Jaffe, W. C. Jones, A. Karakci, E. Keihänen, R. Keskitalo, K. Kiiveri, J. Kim, T. S. Kisner, L. Knox, N. Krachmalnicoff, M. Kunz, H. Kurki-Suonio, G. Lagache, J. M. Lamarre, A. Lasenby, M. Lattanzi, C. R. Lawrence, M. Le Jeune, P. Lemos, J. Lesgourgues, F. Levrier, A. Lewis, M. Liguori, P. B. Lilje, M. Lilley, V. Lindholm, M. López-Caniego, P. M. Lubin, Y. Z. Ma, J. F. Macías-Pérez, G. Maggio, D. Maino, N. Mandolesi, A. Mangilli, A. Marcos-Caballero, M. Maris, P. G. Martin, M. Martinelli, E. Martínez-González, S. Matarrese, N. Mauri, J. D. McEwen, P. R. Meinhold, A. Melchiorri, A. Mennella, M. Migliaccio, M. Millea, S. Mitra, M. A. Miville-Deschénes, D. Molinari, L. Montier, G. Morgante, A. Moss, P. Natoli, H. U. Nørgaard-Nielsen, L. Pagano, D. Paoletti, B. Partridge, G. Patanchon, H. V. Peiris, F. Perrotta, V. Pettorino, F. Piacentini, L. Polastri, G. Polenta, J. L. Puget, J. P. Rachen, M. Reinecke, M. Remazeilles, A. Renzi, G. Rocha, C. Rosset, G. Roudier, J. A. Rubiño-Martín, B. Ruiz-Granados, L. Salvati, M. Sandri, M. Savelainen, D. Scott, E. P. S. Shellard, C. Sirignano, G. Sirri, L. D. Spencer, R. Sunyaev, A. S. Suur-Uski, J. A. Tauber, D. Tavagnacco, M. Tenti, L. Toffolatti, M. Tomasi, T. Trombetti, L. Valenziano, J. Valiviita, B. Van Tent, L. Vibert, P. Vielva, F. Villa, N. Vittorio, B. D. Wandelt, I. K. Wehus, M. White, S. D. M. White, A. Zacchei, and A. Zonca, *Planck 2018 results. VI. Cosmological parameters*, arXiv e-prints (July, 2018) arXiv:1807.06209, [[arXiv:1807.06209](https://arxiv.org/abs/1807.06209)].

[10] Y. Feng, M.-Y. Chu, U. Seljak, and P. McDonald, *FastPM: Scaling N-body Particle Mesh solver*, May, 2019.

[11] N. Hand, Y. Feng, F. Beutler, Y. Li, C. Modi, U. Seljak, and Z. Slepian, *nbodykit: An Open-source, Massively Parallel Toolkit for Large-scale Structure*, *AJ* **156** (Oct, 2018) 160, [[arXiv:1712.05834](https://arxiv.org/abs/1712.05834)].

[12] DESI Collaboration, A. Aghamousa, J. Aguilar, S. Ahlen, S. Alam, L. E. Allen, C. Allende Prieto, J. Annis, S. Bailey, C. Balland, and et al., *The DESI Experiment Part I: Science, Targeting, and Survey Design*, ArXiv e-prints (Oct., 2016) [[arXiv:1611.00036](https://arxiv.org/abs/1611.00036)].

[13] D. Schlegel, J. A. Kollmeier, and S. Ferraro, *The MegaMapper: a $z > 2$ spectroscopic instrument for the study of Inflation and Dark Energy*, in *Bulletin of the AAS*, vol. 51, p. 229, Sept., 2019. [arXiv:1907.11171](https://arxiv.org/abs/1907.11171).

[14] The MSE Science Team, C. Babusiaux, M. Bergemann, A. Burgasser, S. Ellison, D. Haggard, D. Huber, M. Kaplinghat, T. Li, J. Marshall, S. Martell, A. McConnachie, W. Percival, A. Robotham, Y. Shen, S. Thirupathi, K.-V. Tran, C. Yeche, D. Yong, V. Adibekyan, V. Silva Aguirre, G. Angelou, M. Asplund, M. Balogh, P. Banerjee, M. Bannister, D. Barria, G. Battaglia, A. Bayo, K. Bechtol, P. G. Beck, T. C. Beers, E. P. Bellinger, T. Berg, J. M. Bestenlehner, M. Bilicki, B. Bitsch, J. Bland-Hawthorn, A. S. Bolton, A. Boselli, J. Bovy, A. Bragaglia, D. Buzasi, E. Caffau, J. Cami, T. Carleton, L. Casagrande, S. Cassisi, M. Catelan, C. Chang, L. Cortese, I. Damjanov, L. J. M. Davies, R. de Grijs, G. de Rosa, A. Deason, P. di Matteo, A. Drlica-Wagner, D. Erkal, A. Escorza, L. Ferrarese, S. W. Fleming, A. Font-Ribera, K. Freeman, B. T. Gansicke, M. Gabdeev, S. Gallagher, D. Gandolfi, R. A. Garcia, P. Gaulme, M. Geha, M. Gennaro, M. Gieles, K. Gilbert, Y. Gordon, A. Goswami, J. P. Greco, C. Grillmair, G. Guiglion, V. Hénault-Brunet, P. Hall, G. Handler, T. Hansen, N. Hathi, D. Hatzidimitriou, M. Haywood, J. V. Hernández Santisteban, L. Hillenbrand, A. M. Hopkins, C. Howlett, M. J. Hudson, R. Ibata, D. Ilić, P. Jablonka, A. Ji, L. Jiang, S. Juneau, A. Karakas, D. Karinkuzhi, S. Y. Kim, X. Kong, I. Konstantopoulos, J.-K. Krogager, C. Lagos, R. Lallement, C. Laporte, Y. Lebreton, K.-G. Lee, G. F. Lewis, S. Lianou, X. Liu, N. Lodieu, J. Loveday, S. Mészáros, M. Makler, Y.-Y. Mao, D. Marchesini, N. Martin, M. Mateo, C. Melis, T. Merle, A. Miglio, F. Gohar Mohammad, K. Molaverdikhani, R. Monier, T. Morel, B. Mosser, D. Nataf, L. Necib, H. R. Neilson, J. A. Newman, A. M. Nierenberg, B. Nord, P. Noterdaeme, C. O'Dea, M. Oshagh, A. B. Pace, N. Palanque-Delabrouille, G. Pandey, L. C. Parker, M. S. Pawlowski, A. H. G. Peter, P. Petitjean, A. Petric, V. Placco, L. Č. Popović, A. M. Price-Whelan, A. Prsa, S. Ravindranath, R. M. Rich, J. Ruan, J. Rybizki, C. Sakari, R. E. Sanderson, R. Schiavon, C. Schmid, A. Serenelli, A. Siebert, M. Siudek, R. Smiljanic, D. Smith, J. Sobeck, E. Starkenburg, D. Stello, G. M. Szabó, R. Szabo, M. A. Taylor, K. Thanjavur, G. Thomas, E. Tollerud, S. Toonen, P.-E. Tremblay, L. Tresse, M. Tsantaki, M. Valentini, S. Van Eck, A. Variu, K. Venn, E. Villaver, M. G. Walker, Y. Wang, Y. Wang, M. J. Wilson, N. Wright, S. Xu, M. Yıldız, H. Zhang, K. Zwintz, B. Anguiano, M. Bedell, W. Chaplin, R. Collet, J.-C. Cuillandre, P.-A. Duc, N. Flagey, J. Hermes, A. Hill, D. Kamath, M. B. Laychak, K. Małek, M. Marley, A. Sheinis, D. Simons, S. G. Sousa, K. Szeto, Y.-S. Ting, S. Vegetti, L. Wells, F. Babas, S. Bauman, A. Bosselli, P. Côté, M. Colless, J. Comparat, H. Courtois, D. Crampton, S. Croom, L. Davies, R. de Grijs, K. Denny, D. Devost, P. di Matteo, S. Driver, M. Fernandez-Lorenzo, R. Guhathakurta, Z. Han, C. Higgs, V. Hill, K. Ho, A. Hopkins, M. Hudson, R. Ibata, S. Isani, M. Jarvis, A. Johnson, E. Jullo, N. Kaiser, J.-P. Kneib, J. Koda, G. Koshy, S. Mignot, R. Murowinski, J. Newman, A. Nusser, A. Pancoast, E. Peng, C. Peroux, C. Pichon, B. Poggianti, J. Richard, D. Salmon, A. Seibert, P. Shastri, D. Smith, F. Sutaria, C. Tao, E. Taylor, B. Tully, L. van Waerbeke, T. Vermeulen, M. Walker, J. Willis, C. Willot, and K. Withington, *The Detailed Science Case for the Maunakea Spectroscopic Explorer, 2019 edition*, arXiv e-prints (Apr., 2019) arXiv:1904.04907, [[arXiv:1904.04907](https://arxiv.org/abs/1904.04907)].

[15] A. Slosar, Z. Ahmed, D. Alonso, M. A. Amin, E. J. Arena, K. Bandura, N. Battaglia, J. Blazek, P. Bull, E. Castorina, T.-C. Chang, L. Connor, R. Davé, C. Dvorkin, A. van Engelen, S. Ferraro, R. Flauger, S. Foreman, J. Frisch, D. Green, G. Holder, D. Jacobs, M. C. Johnson, J. S. Dillon, D. Karagiannis, A. A. Kaurov, L. Knox, A. Liu, M. Loverde, Y.-Z. Ma, K. W. Masui, T. McClintock, K. Moodley, M. Munchmeyer, L. B. Newburgh, C. Ng, A. Nomerotski, P. O'Connor, A. Obuljen, H. Padmanabhan, D. Parkinson, J. X. Prochaska, S. Rajendran, D. Rapetti, B. Saliwanchik, E. Schaan, N. Sehgal, J. R. Shaw, C. Sheehy, E. Sheldon, R. Shirley, E. Silverstein, T. Slatyer, A. Slosar, P. Stankus, A. Stebbins, P. T. Timbie, G. S. Tucker, W. Tyndall, F. Villaescusa Navarro, B. Wallisch, and M. White, *Packed Ultra-wideband Mapping Array (PUMA): A Radio Telescope for Cosmology and Transients*, in *Bulletin of the AAS*, vol. 51, p. 53, Sep. 2019. [arXiv:1907.12559](https://arxiv.org/abs/1907.12559).

- [16] J. Adams, B. Cresswell, and R. Easter, *Inflationary perturbations from a potential with a step*, *PRD* **64** (Dec., 2001) 123514, [[astro-ph/0102236](#)].
- [17] J. C. Hill, E. McDonough, M. W. Toomey, and S. Alexander, *Early Dark Energy Does Not Restore Cosmological Concordance*, *arXiv e-prints* (Mar., 2020) arXiv:2003.07355, [[arXiv:2003.07355](#)].
- [18] M. M. Ivanov, E. McDonough, J. C. Hill, M. Simonović, M. W. Toomey, S. Alexander, and M. Zaldarriaga, *Constraining Early Dark Energy with Large-Scale Structure*, *arXiv e-prints* (June, 2020) arXiv:2006.11235, [[arXiv:2006.11235](#)].
- [19] G. D'Amico, L. Senatore, P. Zhang, and H. Zheng, *The Hubble Tension in Light of the Full-Shape Analysis of Large-Scale Structure Data*, *arXiv e-prints* (June, 2020) arXiv:2006.12420, [[arXiv:2006.12420](#)].
- [20] A. Klypin, V. Poulin, F. Prada, J. Primack, M. Kamionkowski, V. Avila-Reese, A. Rodriguez-Puebla, P. Behroozi, D. Hellinger, and T. L. Smith, *Clustering and Halo Abundances in Early Dark Energy Cosmological Models*, *arXiv e-prints* (June, 2020) arXiv:2006.14910, [[arXiv:2006.14910](#)].
- [21] D. Blas, J. Lesgourgues, and T. Tram, *The Cosmic Linear Anisotropy Solving System (CLASS). Part II: Approximation schemes*, *JCAP* **7** (July, 2011) 034, [[arXiv:1104.2933](#)].
- [22] S. Bharadwaj, *The Evolution of Correlation Functions in the Zeldovich Approximation and Its Implications for the Validity of Perturbation Theory*, *ApJ* **472** (Nov., 1996) 1–+, [[astro-ph/9](#)].
- [23] T. Matsubara, *Resumming cosmological perturbations via the Lagrangian picture: One-loop results in real space and in redshift space*, *PRD* **77** (Mar., 2008) 063530, [[arXiv:0711.2521](#)].
- [24] T. Matsubara, *Nonlinear perturbation theory with halo bias and redshift-space distortions via the Lagrangian picture*, *PRD* **78** (Oct., 2008) 083519, [[arXiv:0807.1733](#)].
- [25] D. J. Eisenstein, H.-J. Seo, and M. White, *On the Robustness of the Acoustic Scale in the Low-Redshift Clustering of Matter*, *ApJ* **664** (Aug., 2007) 660–674, [[astro-ph/0604361](#)].
- [26] N. Padmanabhan, M. White, and J. D. Cohn, *Reconstructing baryon oscillations: A Lagrangian theory perspective*, *PRD* **79** (Mar., 2009) 063523, [[arXiv:0812.2905](#)].
- [27] Y. Noh, M. White, and N. Padmanabhan, *Reconstructing baryon oscillations*, *PRD* **80** (Dec., 2009) 123501, [[arXiv:0909.1802](#)].
- [28] J. Carlson, B. Reid, and M. White, *Convolution Lagrangian perturbation theory for biased tracers*, *MNRAS* **429** (Feb., 2013) 1674–1685, [[arXiv:1209.0780](#)].
- [29] S. Tasseev and M. Zaldarriaga, *Towards an optimal reconstruction of baryon oscillations*, *JCAP* **10** (Oct., 2012) 006, [[arXiv:1203.6066](#)].
- [30] N. McCullagh and A. S. Szalay, *Nonlinear Behavior of Baryon Acoustic Oscillations from the Zel'dovich Approximation Using a Non-Fourier Perturbation Approach*, *ApJ* **752** (June, 2012) 21, [[arXiv:1202.1306](#)].
- [31] M. White, *The Zel'dovich approximation*, *MNRAS* **439** (Apr., 2014) 3630–3640, [[arXiv:1401.5466](#)].
- [32] Z. Vlah, U. Seljak, M. Yat Chu, and Y. Feng, *Perturbation theory, effective field theory, and oscillations in the power spectrum*, *JCAP* **2016** (Mar, 2016) 057, [[arXiv:1509.02120](#)].
- [33] M. McQuinn and M. White, *Cosmological perturbation theory in 1+1 dimensions*, *JCAP* **1** (Jan., 2016) 043, [[arXiv:1502.07389](#)].
- [34] M. Crocce and R. Scoccimarro, *Nonlinear evolution of baryon acoustic oscillations*, *PRD* **77** (Jan., 2008) 023533, [[arXiv:0704.2783](#)].

[35] L. Senatore and M. Zaldarriaga, *The IR-resummed Effective Field Theory of Large Scale Structures*, *JCAP* **2** (Feb., 2015) 13, [[arXiv:1404.5954](https://arxiv.org/abs/1404.5954)].

[36] M. Schmittfull, Y. Feng, F. Beutler, B. Sherwin, and M. Y. Chu, *Eulerian BAO reconstructions and N-point statistics*, *PRD* **92** (Dec., 2015) 123522, [[arXiv:1508.06972](https://arxiv.org/abs/1508.06972)].

[37] T. Baldauf, M. Mirbabayi, M. Simonović, and M. Zaldarriaga, *Equivalence principle and the baryon acoustic peak*, *PRD* **92** (Aug., 2015) 043514, [[arXiv:1504.04366](https://arxiv.org/abs/1504.04366)].

[38] D. Blas, M. Garny, M. M. Ivanov, and S. Sibiryakov, *Time-sliced perturbation theory II: baryon acoustic oscillations and infrared resummation*, *JCAP* **2016** (July, 2016) 028, [[arXiv:1605.02149](https://arxiv.org/abs/1605.02149)].

[39] H.-J. Seo, F. Beutler, A. J. Ross, and S. Saito, *Modeling the reconstructed BAO in Fourier space*, *MNRAS* **460** (Aug., 2016) 2453–2471, [[arXiv:1511.00663](https://arxiv.org/abs/1511.00663)].

[40] Z. Ding, H.-J. Seo, Z. Vlah, Y. Feng, M. Schmittfull, and F. Beutler, *Theoretical systematics of Future Baryon Acoustic Oscillation Surveys*, *MNRAS* **479** (Sept., 2018) 1021–1054, [[arXiv:1708.01297](https://arxiv.org/abs/1708.01297)].

[41] C. Hikage, K. Koyama, and A. Heavens, *Perturbation theory for BAO reconstructed fields: One-loop results in the real-space matter density field*, *PRD* **96** (Aug., 2017) 043513, [[arXiv:1703.07878](https://arxiv.org/abs/1703.07878)].

[42] M. Peloso and M. Pietroni, *Galilean invariant resummation schemes of cosmological perturbations*, *JCAP* **2017** (Jan., 2017) 056, [[arXiv:1609.06624](https://arxiv.org/abs/1609.06624)].

[43] M. M. Ivanov and S. Sibiryakov, *Infrared resummation for biased tracers in redshift space*, *JCAP* **2018** (July, 2018) 053, [[arXiv:1804.05080](https://arxiv.org/abs/1804.05080)].

[44] A. Vasudevan, M. M. Ivanov, S. Sibiryakov, and J. Lesgourgues, *Time-sliced perturbation theory with primordial non-Gaussianity and effects of large bulk flows on inflationary oscillating features*, *JCAP* **2019** (Sept., 2019) 037, [[arXiv:1906.08697](https://arxiv.org/abs/1906.08697)].

[45] M. Ballardini, R. Murgia, M. Baldi, F. Finelli, and M. Viel, *Non-linear damping of superimposed primordial oscillations on the matter power spectrum in galaxy surveys*, *JCAP* **2020** (Apr., 2020) 030, [[arXiv:1912.12499](https://arxiv.org/abs/1912.12499)].

[46] S.-F. Chen, Z. Vlah, and M. White, *Consistent Modeling of Velocity Statistics and Redshift-Space Distortions in One-Loop Perturbation Theory*, *arXiv e-prints* (May, 2020) arXiv:2005.00523, [[arXiv:2005.00523](https://arxiv.org/abs/2005.00523)].

[47] T. Lazeyras, M. Musso, and V. Desjacques, *Lagrangian bias of generic large-scale structure tracers*, *PRD* **93** (Mar., 2016) 063007, [[arXiv:1512.05283](https://arxiv.org/abs/1512.05283)].

[48] M. M. Abidi and T. Baldauf, *Cubic halo bias in Eulerian and Lagrangian space*, *JCAP* **2018** (July, 2018) 029, [[arXiv:1802.07622](https://arxiv.org/abs/1802.07622)].

[49] Z. Vlah and M. White, *Exploring redshift-space distortions in large-scale structure*, *JCAP* **2019** (Mar, 2019) 007, [[arXiv:1812.02775](https://arxiv.org/abs/1812.02775)].

[50] B. A. Reid and M. White, *Towards an accurate model of the redshift-space clustering of haloes in the quasi-linear regime*, *MNRAS* **417** (Nov., 2011) 1913–1927, [[arXiv:1105.4165](https://arxiv.org/abs/1105.4165)].

[51] Z. Vlah, E. Castorina, and M. White, *The Gaussian streaming model and convolution Lagrangian effective field theory*, *JCAP* **12** (Dec., 2016) 007, [[arXiv:1609.02908](https://arxiv.org/abs/1609.02908)].